

# Simultaneous fitting of statistical-model parameters to symmetric and asymmetric fission cross sections

D Mancusi<sup>1</sup>, R J Charity<sup>2</sup> and J Cugnon<sup>3</sup>

<sup>1</sup> CEA, Centre de Saclay, Irfu/Service de Physique Nucléaire, F-91191 Gif-sur-Yvette, France

<sup>2</sup> Department of Chemistry, Washington University, St. Louis, Missouri 63130, USA

<sup>3</sup> University of Liège, AGO Department, allée du 6 Août 17, bât. B5, B-4000 Liège 1, Belgium

E-mail: [davide.mancusi@cea.fr](mailto:davide.mancusi@cea.fr)

**Abstract.** The de-excitation of compound nuclei has been successfully described for several decades by means of statistical models. However, accurate predictions require some fine-tuning of the model parameters. This task can be simplified by studying several entrance channels, which populate different regions of the parameter space of the compound nucleus.

Fusion reactions play an important role in this strategy because they minimise the uncertainty on the entrance channel by fixing mass, charge and excitation energy of the compound nucleus. If incomplete fusion is negligible, the only uncertainty on the compound nucleus comes from the spin distribution. However, some de-excitation channels, such as fission, are quite sensitive to spin. Other entrance channels can then be used to discriminate between equivalent parameter sets.

The focus of this work is on fission and intermediate-mass-fragment emission cross sections of compound nuclei with  $70 \lesssim A \lesssim 240$ . The statistical de-excitation model is GEMINI++. The choice of the observables is natural in the framework of GEMINI++, which describes fragment emission using a fission-like formalism. Equivalent parameter sets for fusion reactions can be resolved using the spallation entrance channel. This promising strategy can lead to the identification of a minimal set of physical ingredients necessary for a unified quantitative description of nuclear de-excitation.

## 1. Introduction

The de-excitation of an excited nucleus is a qualitatively well-understood phenomenon which is often described by means of statistical models. However, such models contain a great deal of free parameters and ingredients that are often underconstrained by the available experimental data. Quantitatively accurate predictions usually require some tuning of the model parameters.

The fusion entrance channel is a particularly powerful tool to explore the sensitivity of the de-excitation model to the compound-nucleus parameters (mass, charge, excitation energy and spin); if the cross sections for incomplete fusion and pre-equilibrium emission are negligible with respect to the fusion cross section for a given projectile-target combination, the compound nucleus can essentially be regarded as having a fixed mass, charge and total excitation energy (intrinsic plus collective), thereby fixing three of the four parameters that describe it. The requirement of complete fusion, however, puts an upper limit on the energy of the projectile and, thus, on the excitation energies that can be studied with this method. Because of this and other similar limitations on the entrance channel, one is actually able to construct different parameter sets that can describe the same experimental data to a similar degree of accuracy; in this sense, statistical de-excitation models contain partly degenerate ingredients, and that limits their predictive power.

Part of the degeneracy can be removed by performing simultaneous fits to heterogeneous data sets. For example, one can try to explore diverse regions of the compound-nucleus parameter space by studying different reaction entrance channels. The present work combines the fusion and the spallation entrance channels for the study of fission and emission of intermediate-mass fragments (IMFs). The goal is to put more stringent constraints on the de-excitation-model parameters than those that would be obtained from the separate study of fusion- and spallation-induced de-excitation chains.

## 2. Tools

This work focuses on the GEMINI++ nuclear de-excitation model [1]. One of the most prominent features of GEMINI++ is that it accurately models changes in orbital and intrinsic angular momentum of the de-excitation products along the de-excitation chain. This is particularly important for the study of fission and IMF emission, which are quite sensitive to the spin of the mother nucleus.

For nuclides above the Businaro-Gallone point, the ridge of conditional saddle points as a function of the asymmetry of the split exhibits a minimum around symmetric splitting and two local maxima on either side (apart from local variations due to structure effects). For such systems, GEMINI++ adopts a global description of fission. The statistical width of the process is computed using a Bohr-Wheeler-type formalism, with barriers taken from Sierk's finite-range calculations [2, 3]. In addition, several corrections are possible within the framework of the model: (a) different level-density parameters at the saddle point and in the ground state, (b) a constant shift of the Sierk barrier heights, (c) overall scaling of the fission width, and (d) explicit treatment of the tilting degree of freedom at saddle [4]. This establishes the free ingredients of our fission model. The scission mass and charge distributions are taken from Rusanov *et al*'s systematics [5].

GEMINI++ also considers the emission of fragments with  $3 < A < A_{\text{IMF}}$ , where  $A_{\text{IMF}}$  is the fragment mass corresponding to the first maximum in the ridge of conditional saddle points. This process is also described by a transition-state formalism [6], with explicitly singled-out mass- and charge-asymmetry degrees of freedom at saddle. Given the formal similarity, the IMF-emission model includes the same free ingredients as the fission model. Finally, the emission of nucleons and light clusters ( $A \leq 3$ ) is described by the Hauser-Feshbach evaporation formalism [7].

### 2.1. Models for the entrance channel

Besides the de-excitation model, the proposed task requires models for the reaction entrance channels. For fusion, we limit our study to incident energies lower than about 10 A MeV, where incomplete fusion and pre-equilibrium should be negligible; thus, we only need to specify the spin distribution of the compound nucleus. We assume the following roughly triangular shape:

$$\sigma_{\text{fus}}(J) = \pi \lambda^2 (2J + 1) \left[ 1 + \exp\left(\frac{J - J_0}{\Delta J}\right) \right]^{-1},$$

where  $J_0$  determines the maximum spin value and  $\Delta J$  plays the role of a smooth cutoff. The  $J_0$  parameter is fixed from the total fusion cross section

$$\sigma_{\text{fus}} = \sum_{J=0}^{\infty} \sigma_{\text{fus}}(J),$$

while  $\Delta J$  is set to values from 3 to 10  $\hbar$ , with the larger values associated with the heavier projectiles. For the reactions for which we present IMF data, the fusion cross sections have not been measured and the Friction model [8] or the Extra-Push model [9] were used to calculate both the cross sections and maximum spin values.

The entrance channel for spallation reactions is described by the Liège Intranuclear-Cascade model (INCL) [10]. In this framework, the high-energy incident nucleon initiates an avalanche of binary

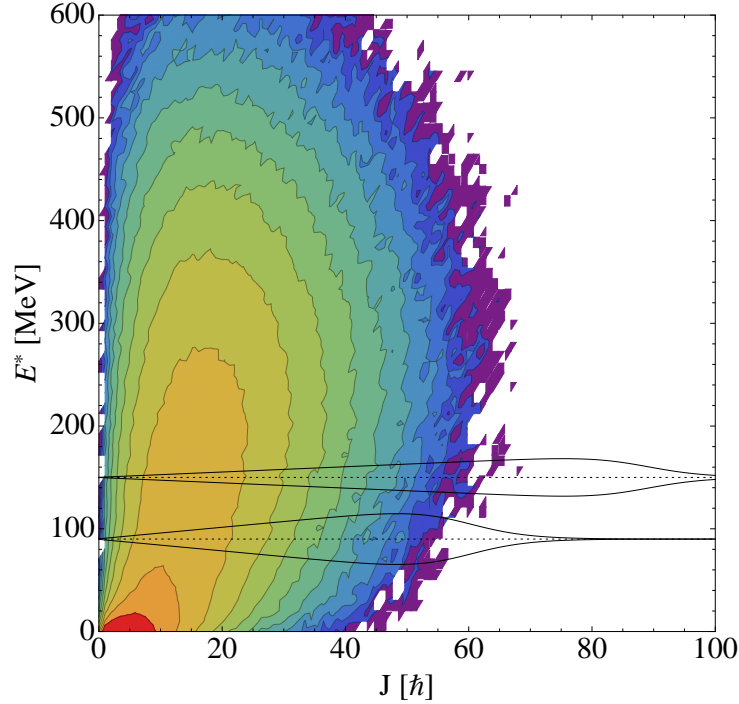


**Figure 1.** Comparison of the distributions of excitation energy and spin populated in the  $^{19}\text{F}+^{181}\text{Ta}\rightarrow^{200}\text{Pb}$  fusion reaction for  $E^* = 90, 150$  MeV (horizontal lines) with the INCL prediction for the 1-GeV  $p+^{208}\text{Pb}$  spallation reaction (contours, logarithmically spaced).

nucleon-nucleon collisions within the target nucleus, which can lead to the emission of a few nucleons and possibly pions. The cascade is stopped when the cascade remnant shows signs of thermalisation. This provides the entry point for the GEMINI++ de-excitation chain. A more comprehensive description of the latest INCL developments has been recently published [11]. One should stress here that the INCL model does have internal parameters, but they have been either taken from known phenomenology (e.g. the parameters describing nuclear density distributions) or fixed once and for all (e.g. the parameters connected with the description of Pauli collision blocking). Thus, the present work only focuses on the adjustment of the GEMINI++ side of the reaction model.

The validity of the INCL model in the 50-MeV to 3-GeV incident-energy range has been extensively demonstrated by the recent “Benchmark of Spallation Models” [12, 13], sponsored by IAEA. We assume that INCL provides an accurate description of the initial stage of spallation reactions within the energy range above. Above 3 GeV, the model is known to be less reliable [14]. This limits the pool of experimental data that can be considered if we require that the entrance-channel model should not introduce considerable uncertainty on the model predictions.

## 2.2. Complementarity of fusion and spallation

Figure 1 illustrates how spallation and fusion reactions efficiently complement each other in probing the parameter space of thermalised nuclei. Spallation reactions produce broad distributions of excited nuclei, whose projection on the spin/excitation-energy plane is represented by the coloured contours. Rather high excitation energies can be realised, but spin is limited to a few tens of  $\hbar$ . This complements well the limitations of fusion reactions, which are represented by the horizontal shapes. The width of the shapes is proportional to the spin distributions of the  $^{19}\text{F}+^{181}\text{Ta}\rightarrow^{200}\text{Pb}$  fusion reaction, for two different excitation energies.

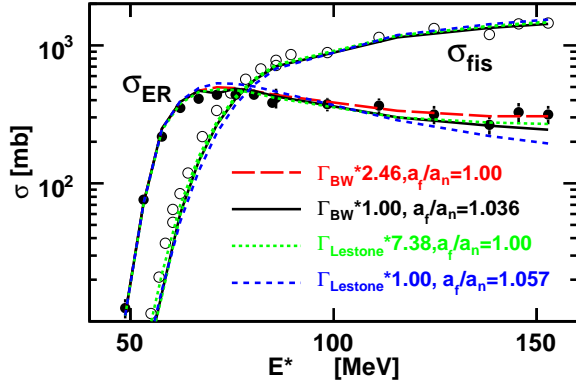


**Figure 2.** Experimental [15, 16] and calculated GEMINI++ predictions for evaporation-residue and fission excitation functions for the  $^{19}\text{F}+^{181}\text{Ta}$  reaction.

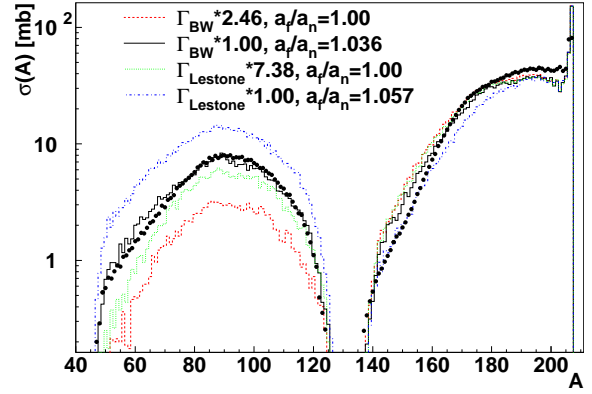


**Figure 3.** Experimental [17] and calculated residual mass distributions for the 1-GeV  $p+^{208}\text{Pb}$  reaction.

### 3. Results for fission

We first discuss fusion-fission and spallation-fission calculations for compound nuclei of similar mass and charge. Figure 2 shows the result of four fits to fusion-fission data: here  $\Gamma_{\text{BW}}$  and  $\Gamma_{\text{Lestone}}$  indicate calculations performed without or with Lestone's tilting correction, respectively; a global scaling factor is applied in some parameter sets; and  $a_f/a_n$  represents the ratio of the level-density parameters at saddle and in the ground-state (assumed to be a constant). The degeneracy of the four parameter sets is clearly illustrated. However, the application of the same parameter sets to spallation-fission reactions largely lifts the degeneracy for this observable, as shown in Figure 3.

The combined fusion/spallation approach allowed us to construct predictive parameter sets for fission and evaporation-residue excitation curves in the compound-nucleus mass range  $155 \lesssim A \lesssim 225$  [18]. The agreement with experimental data for both types of reactions was in general very good, apart from some overestimation of fission cross sections for the lightest compound nuclei ( $A < 170$ ).

### 4. Results for IMF emission

We now proceed to illustrate the application of the same strategy to fragment charge distributions from non-fissile compound nuclei, which cover IMF-production cross sections. Given the paucity of available data, we also considered experimental data for reactions above 10 AMeV incident energy, for which incomplete fusion might not be negligible. In all cases, however, the authors of the experimental papers state that the incomplete-fusion component has been properly subtracted.

#### 4.1. Fusion reactions

Figure 4 shows the charge distribution of fragments obtained from  $^{58}\text{Ni}+^{12}\text{C} \rightarrow ^{76}\text{Se}$  fusion at 6.63 and 12.95 AMeV incident energy. The figure illustrates the sensitivity of the calculation results to three parameters: a constant shift of the Sierk IMF barriers ( $\Delta B$ ), the saddle-to-ground-state ratio of level-density parameters ( $a_{\text{IMF}}/a_n$ , analogous to the  $a_f/a_n$  parameter for fission) and the diffuseness parameter of the spin distribution ( $\Delta J$ ). IMF yields from fusion show great sensitivity to the barrier height, which is expected because the compound-nucleus nuclear temperature ( $T \sim$  a few MeV) is much smaller than the typical IMF barrier height ( $B \sim$  a few tens of MeV) and the transition rate scales approximately as  $\exp(-B/T)$ . For the same reason, IMF yields from fusion are relatively insensitive to the small variation of the  $a_{\text{IMF}}/a_n$  ratio, which determines the temperature  $T$ . The diffuseness of the spin distribution also has some effect on the IMF yields, especially at low excitation energy. We observe that the experimental

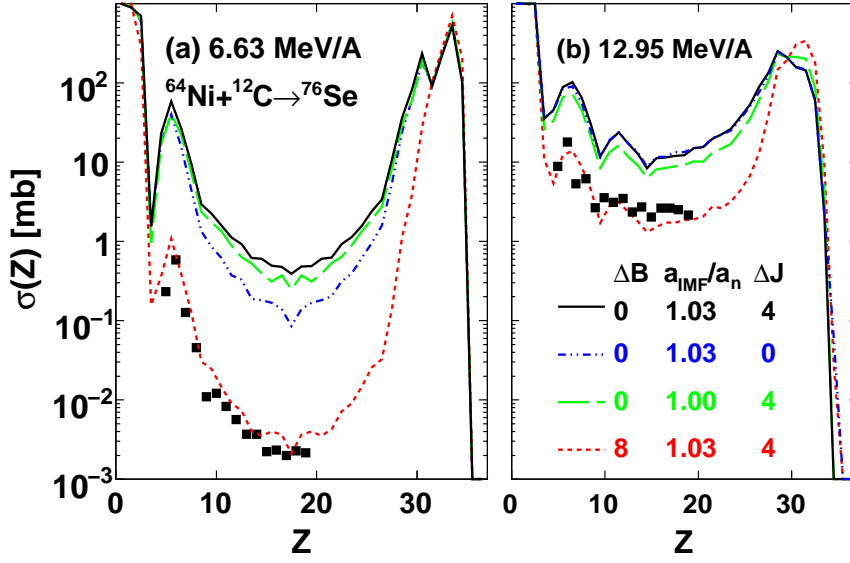


**Figure 4.** Comparison of the experimental charge distribution for the (a)  $E/A = 6.63$  MeV and (b)  $E/A = 12.95$  MeV  $^{64}\text{Ni} + ^{12}\text{C} \rightarrow ^{76}\text{Se}$  fusion reaction with calculation with the indicated input parameters. The fusion cross section is given by the Friction model.

data for this system can be satisfactorily reproduced only by adding a shift of 8.5 MeV to Sierk's barriers. Moreover, the data do not show any clear need for an asymmetry dependence of the barrier shift.

Figure 5 shows how IMF-production cross sections from another fusion reaction ( $^{86}\text{Kr} + ^{12}\text{C} \rightarrow ^{98}\text{Mo}$ ) can be accurately described at several excitation energies by applying an asymmetry-independent shift of 7 MeV to the Sierk barriers. The insensitivity of the model predictions to the fusion-cross-section model is also illustrated by the comparison of the Friction and Extra-Push models.

Following this approach, we have fitted barrier shifts to all the available data sets [19, 20, 21, 22, 23]. All charge distributions were fitted with  $a_{\text{IMF}}/a_n = 1.03$  and by varying the quantity  $\Delta B$ . The choice of  $a_{\text{IMF}}/a_n$  will be discussed below (Sec. 4.2), but it is generally not very important for the considered fusion reactions.

The fitted barrier shifts correlate well with the fissility parameter  $Z^2/A$  of the compound nucleus, as shown in Figure 6. The circular data points are from fits to IMF charge distributions.

As mentioned above (Sec. 3), fission cross sections for the lightest compound nuclei were slightly overestimated by our global fission fits [18]. The quality of the fit to fission excitation curves can be improved by increasing the fission barriers by a few MeV. The best-fit shifts are represented by the square data points on Figure 6 and seem to align with the trend shown by the IMF charge distributions. The line shows a linear fit to the red and blue data points.

The physical interpretation of the barrier shift is unclear. The triangular data points on Figure 6 represent differences between Sierk's finite-range barriers and the Rotating Liquid-Drop barriers [24], which are mainly due to the finite-range and surface-diffuseness corrections included in Sierk's model. The dependence on  $Z^2/A$  is similar to our barrier shifts. This might indicate that Sierk's model overestimates the extent of the correction.

One can also try to explain the barrier shift as an effect of the deformation dependence of the Wigner energy of the mother nucleus [25]. However, if this interpretation were correct, the barrier shifts should show some dependence on  $|N - Z|/A$ , the asymmetry parameter of the compound nucleus, with a minimum close to symmetry. No clear trend appears on Figure 7. Thus, the physical meaning of the barrier shift remains ambiguous.

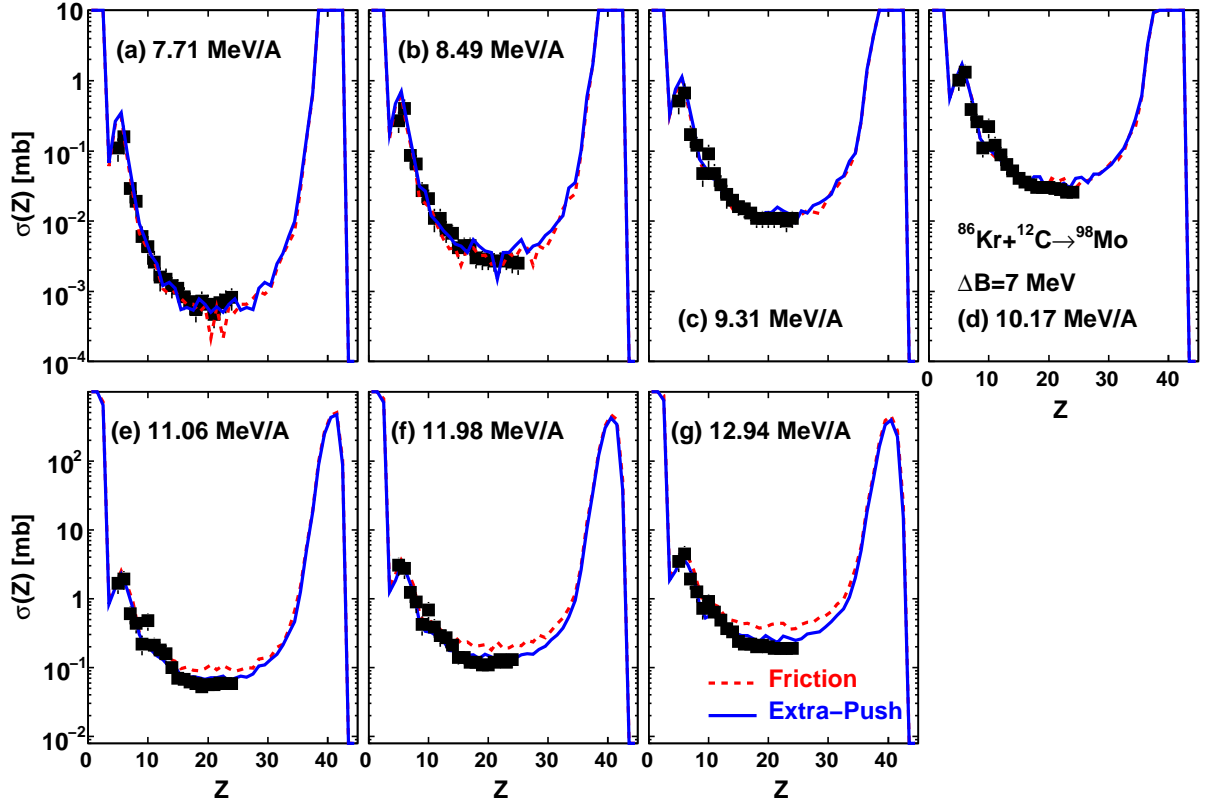


**Figure 5.** Comparison of experimental and fitted charge distributions for the  $^{86}\text{Kr}+^{12}\text{C}$  reaction.

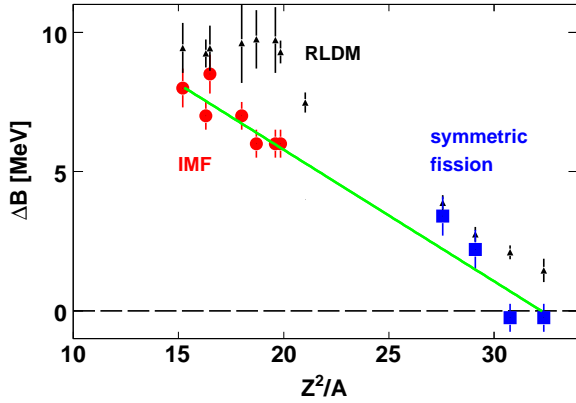


**Figure 6.** Shifts to the finite-range barriers  $\Delta B$  needed to fit data, plotted as a function of the  $Z^2/A$  of the compound nucleus.

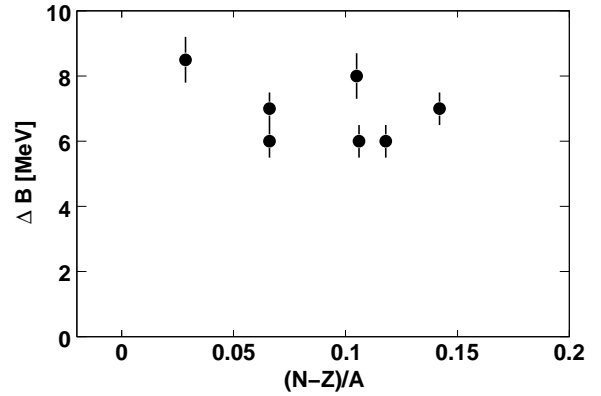


**Figure 7.** Shifts to the finite-range barriers  $\Delta B$  needed to fit the experimental IMF charge distributions, plotted as a function of the asymmetry parameter.

#### 4.2. Spallation reactions

Accurate measurements of IMF charge distributions from spallation reactions below 3 GeV are even more scarce than measurements for fusion reactions. Moreover, there is some controversy over IMF production cross sections from 1-GeV  $p+^{136}\text{Xe}$  system; the two existing measurements [26, 27] disagree of about a factor of 3 for  $10 \lesssim Z \lesssim 30$ . This situation prevents us from providing a unique, predictive

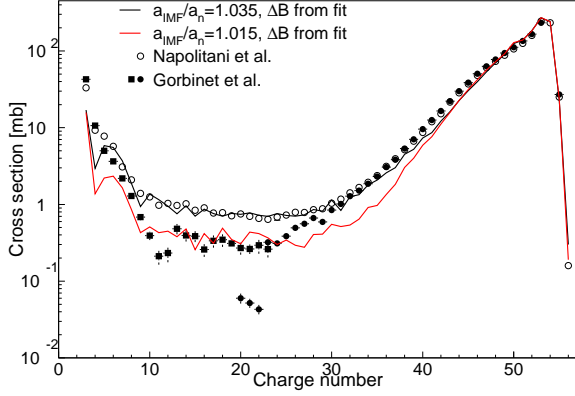


**Figure 8.** Experimental [26, 27] and calculated residual charge distributions for 1-GeV p+<sup>136</sup>Xe. The two symbols for Gorbinet *et al.* 's data correspond to different techniques (see text for more details).

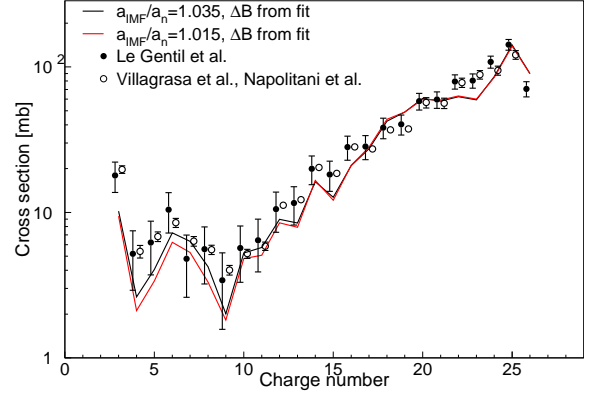


**Figure 9.** Experimental [28, 29, 30] and calculated residual charge distributions for 1-GeV p+<sup>56</sup>Fe.

parameter set that can simultaneously describe IMF data from fusion and spallation reactions.

Note that Gorbnet *et al.* 's cross sections in Figure 8 actually consist of two separate data sets. The filled squares for  $Z \leq 23$  represent actual fragment-production cross sections. The filled circles for  $Z \geq 20$  represent cross sections as a function of  $Z_{\max}$ , the largest charge produced in an event. For  $Z > 27$ , the  $Z_{\max}$  cross sections must be equal to the fragment-production cross sections, since  $Z > 27$  fragments are always the largest charges in the events that involve them. For  $Z \leq 27$ , the actual fragment-production cross sections may be larger than the  $Z_{\max}$  cross sections, if fragments are sometimes produced in coincidence with larger partners. The two techniques however yield comparable cross sections for  $Z = 23$ , suggesting that such fragments are never accompanied by larger partners. For more details, we refer the reader to Gorbnet's Ph.D. thesis [27].

A linear function of  $Z^2/A$  was fit to the barrier shifts determined from fusion reactions (Figure 6) and applied to all the spallation reactions. Figure 8 shows calculations by INCL/GEMINI++ for the 1-GeV p+<sup>136</sup>Xe system.

It was mentioned above that IMF charge distributions from fusion reactions are rather insensitive to the level-density-parameter ratio  $a_{\text{IMF}}/a_n$ . In spallation reactions, on the contrary, charge distributions exhibit a larger sensitivity to this parameter, due to the higher temperatures attained, as illustrated in Figure 8. The model predicts that fragments with  $10 < Z < 30$  are produced in events with an average excitation energy  $\langle E^* \rangle = 411$  MeV, but the distribution extends up to  $\sim 750$  MeV. We can then conclude that, as in the case of fission, combining fusion and spallation data-sets allows us to lift some of the degeneracy of the model parameters related to IMF production. However, since the available data sets are in disagreement, we provide two best-fit values for the  $a_{\text{IMF}}/a_n$  parameter.

Unfortunately, the 1-GeV p+<sup>56</sup>Fe system does not help to discriminate between the two candidate values of the  $a_{\text{IMF}}/a_n$  parameter. Figure 9 shows that the IMF cross sections are robust against variations of  $a_{\text{IMF}}/a_n$ . Note however that the data are rather accurately described by the model, regardless of the parameter value.

We conclude that IMF production cross sections from fusion and spallation reactions can be accurately described by introducing a  $Z^2/A$ -dependent asymmetric-fission barrier shift and a constant level-density-parameter ratio. The value of the  $a_{\text{IMF}}/a_n$  parameter cannot be fixed until an explanation is found for the 1-GeV p+<sup>136</sup>Xe discrepancy.

## 5. Conclusions

The fusion and spallation entrance channels probe different regions of the compound-nucleus parameter space and can thus be profitably combined to put stringent constraints on some of the free parameters of de-excitation models. We have demonstrated how this strategy can be fruitfully applied to the study of fission and IMF emission.

In particular, we find that we need to increase Sierk's finite-range barriers for IMF emission by a few MeV to fit the data. The best-fit barrier shifts exhibit a phenomenological dependence on  $Z^2/A$  of the compound nucleus which can be fit by a straight line. The description of fission cross sections for compound nuclei with  $A < 170$  ( $Z^2/A \lesssim 30$ ) would also benefit from a slight increase in the barriers. It is unclear whether the barrier shift can be attributed to the deformation dependence of the Wigner energy, because the best-fit barriers appear to be independent of the  $(N - Z)/A$  ratio of the compound nucleus.

Production of IMF from 1-GeV  $p+^{56}\text{Fe}$  and  $^{136}\text{Xe}$  spallation reactions can also be accurately described by the same model, provided that one introduces another free parameter, the ratio of level-density parameters at the conditional saddle point and in the undeformed configuration ( $a_{\text{IMF}}/a_n$ ). Possible values of  $a_{\text{IMF}}/a_n$  range from 1.015 to 1.035, depending on the data sets used for the fit.

## References

- [1] Charity R J 2008 *Joint ICTP-IAEA Advanced Workshop on Model Codes for Spallation Reactions* (Trieste, Italy: IAEA) p 139 report INDC(NDC)-0530
- [2] Sierk A J 1985 *Phys. Rev. Lett.* **55** 582–583
- [3] Carjan N and Alexander J M 1988 *Phys. Rev. C* **38** 1692–1697
- [4] Lestone J P 1999 *Phys. Rev. C* **59** 1540–1544
- [5] Rusanov A Y, Itkis M G and Okolovich V N 1997 *Phys. Atom. Nucl.* **60** 683–712
- [6] Moretto L G 1975 *Nucl. Phys. A* **247** 211–230
- [7] Hauser W and Feshbach H 1952 *Phys. Rev.* **87** 366–373
- [8] Gross D H E and Kalinowski H 1978 *Phys. Rep.* **45** 175–210
- [9] Świątecki W J 1980 *Prog. Part. Nucl. Phys.* **4** 383–450
- [10] Boudard A, Cugnon J, Leray S and Volant C 2002 *Phys. Rev. C* **66** 044615
- [11] Cugnon J, Boudard A, Leray S and Mancusi D 2011 *J. Korean Phys. Soc.* **59** 955–958
- [12] Leray S, David J C, Khandaker M, Mank G, Mengoni A, Otsuka N, Filges D, Gallmeier F, Konobeyev A and Michel R 2011 *J. Korean Phys. Soc.* **59** 791–796
- [13] IAEA benchmark of spallation models official web site URL <http://www-nds.iaea.org/spallations>
- [14] Pedoux S and Cugnon J 2011 *Nucl. Phys. A* **866** 16–36
- [15] Hinde D J, Leigh J R, Newton J O, Galster W and Sie S 1982 *Nucl. Phys. A* **385** 109
- [16] Caraley A L, Henry B P, Lestone J P and Vandenbosch R 2000 *Phys. Rev. C* **62** 054612
- [17] Enqvist T, Wlazło W, Armbruster P, Benlliure J, Bernas M, Boudard A, Czajkowski S, Legrain R, Leray S, Mustapha B, Pravikoff M, Rejmund F, Schmidt K H, Stéphan C, Taïeb J, Tassan-Got L and Volant C 2001 *Nucl. Phys. A* **686** 481–524
- [18] Mancusi D, Charity R J and Cugnon J 2010 *Phys. Rev. C* **82** 044610
- [19] Fan T, Jing K, Phair L, Tso K, McMahan M, Hanold K, Wozniak G and Moretto L 2000 *Nucl. Phys. A* **679** 121–146 ISSN 0375-9474
- [20] Delis D, Blumenfeld Y, Bowman D, Colonna N, Hanold K, Jing K, Justice M, Meng J, Peaslee G, Wozniak G and Moretto L 1991 *Nucl. Phys. A* **534** 403–428 ISSN 0375-9474
- [21] Jing K X, Moretto L G, Veeck A C, Colonna N, Lhenry I, Tso K, Hanold K, Skulski W, Sui Q and Wozniak G J 1999 *Nucl. Phys. A* **645** 203–238



- [22] Sobotka L G, McMahan M A, McDonald R J, Signarbieux C, Wozniak G J, Padgett M L, Gu J H, Liu Z H, Yao Z Q and Moretto L G 1984 *Phys. Rev. Lett.* **53**(21) 2004–2007
- [23] Charity R, McMahan M, Wozniak G, McDonald R, Moretto L, Sarantites D, Sobotka L, Guarino G, Pantaleo A, Fiore L, Gobbi A and Hildenbrand K 1988 *Nucl. Phys. A* **483** 371 – 405 ISSN 0375-9474
- [24] Cohen S, Plasil F and Świątecki W J 1974 *Ann. Phys. (N.Y.)* **82** 557–596
- [25] Myers W D and Świątecki W J 1997 *Nucl. Phys. A* **612** 249–261
- [26] Napolitani P, Schmidt K H, Tassan-Got L, Armbruster P, Enqvist T, Heinz A, Henzl V, Henzlova D, Kelić A, Pleskač R, Ricciardi M V, Schmitt C, Yordanov O, Audouin L, Bernas M, Lafriaskh A, Rejmund F, Stéphan C, Benlliure J, Casarejos E, Fernandez Ordonez M, Pereira J, Boudard A, Fernandez B, Leray S, Villagrasa C and Volant C 2007 *Phys. Rev. C* **76** 064609
- [27] Gorbinet T 2011 *Étude des réactions de spallation  $^{136}\text{Xe}+p$  et  $^{136}\text{Xe}+^{12}\text{C}$  à 1 GeV par nucléon auprès de l'accélérateur GSI (Darmstadt, Allemagne)* Ph.D. thesis Université Paris-Sud 11 Paris, France
- [28] Villagrasa-Canton C *et al.* 2007 *Phys. Rev. C* **75** 044603
- [29] Napolitani P, Schmidt K H, Botvina A S, Rejmund F, Tassan-Got L and Villagrasa C 2004 *Phys. Rev. C* **70** 054607
- [30] Le Gentil E *et al.* 2008 *Phys. Rev. Lett.* **100** 022701